ChemPubSoc
Europe

■ Surface Chemistry

Characterization of a Robust Co^{II} Fluorescent Complex Deposited Intact On HOPG**

María José Heras-Ojea,[a] Daniel Reta Mañeru,[a] Lidia Rosado,[a] Juan Rubio Zuazo,[b] German R. Castro,[b] Subrata Tewary,[c] Gopalan Rajaraman,[c] Guillem Aromí,[a] Erika Jiménez,[b] and E. Carolina Sañudo*[a]

Abstract: The new diimine fluorescent ligand **ACRI-1** based on a central acridine yellow core is reported along with its coordination complex [Co$_2$(**ACRI-1**)$_2$] (**1**), a fluorescent weak ferromagnet. Due to the strong fluorescence of the acridine yellow fluorophore, it is not completely quenched when the ligand is coordinated to Co^{II}. The magnetic properties of bulk complex **1** and its stability in solution have been studied. Complex **1** has been deposited on highly ordered pyro-litic graphite (HOGP) from solution. The thin films prepared have been characterized by AFM, time-of-flight secondary ion mass spectrometry (TOF-SIMS), grazing incidence X-ray diffraction (GIXRD), X-ray absorption spectroscopy (XAS), X-ray magnetic circular dichroism (XMCD) and theoretical calculations. The data show that the complex is robust and remains intact on the surface of graphite.

Introduction

The limit imposed by the superparamagnetic regime present in nanoparticle-based inorganic systems for spintronics sets a miniaturization limit for these systems.[1] At this point, there is a major trend for spintronics: The design of molecular analogues of the inorganic spintronic structures, presenting the possibility of designing cheaper spintronic devices compatible with plastic technology,[2] and the evolution towards molecular spintronics, which takes advantage of the possibility to tailor molecules with control down to the single spin. Basically, these approaches present the following advantages with respect to inorganic spintronics: Electron spins can be preserved for longer times and distances, low density, transparency, chemical versatility, flexibility, processability, and new added functionalities.[3] Since the synthesis of polynuclear complexes does not follow a predictable synthetic method, we have to consider the design inside of the serendipitous assembly process.[4] To attain multifunctional materials, coordination chemistry molecular systems offer the advantage of the possibility of tailoring ligands to carry desired specific functions, like fluorescence, additional to the magnetic properties provided by the transition metal. Additionally, functionalization of the ligands with characteristic chemical groups can also facilitate deposition and organization on surfaces. Thus, different properties can coexist in one same material and be activated by different inputs or there can be synergy between them. The use of multifunctional molecular complexes in the assembly of nanodevices is a hot topic in the fast development of molecular electronics. To include these materials in devices and prior to any possible application, the study of nanostructuration of the prepared systems is of outmost importance.[5] Molecular magnetism is now progressing in this new track, focusing on the organization of nanomagnets in low-dimensional arrays suitable for addressing single molecules. Many efforts are being devoted with this goal in mind; however, the characterization of thin films, monolayers, or sub-monolayers of nanomagnets on surfaces is far from trivial: The amount of material is extremely small and the use of surface sensitive techniques is absolutely necessary. Furthermore, the stability and robustness of the molecular complexes in the deposition conditions must be clearly ascertained. Our group has been interested in nanostructuration of molecular magnets[6] and research efforts are especially being devoted to prepare multifunctional magnetic systems based on molecular species. Gatteschi, Sessoli, and co-workers have addressed this issue in several of their publications, in which deposition methods are surveyed.[7] Winpenny and co-workers have studied the surface deposition of Cr$_7$Ni nanomagnets,[8] with outstanding results. The work on Mn$_{12}$ and Fe$_4$ single-molecule magnets (SMMs) by Sessoli, Sanctiavit, and co-workers has pioneered the use of X-ray absorption (XAS) and X-ray magnetic circular dichroism (XMCD) to characterize thin layers of molecular species on a surface. These studies clearly

[a] M. J. Heras-Ojea, D. R. Mañeru, L. Rosado, Dr. G. Aromí, Dr. E. C. Sañudo
Departament de Química Inorgànica
Facultat de Química, and Institut de Nanociència
i Nanotecnologia IN2UB, Universitat de Barcelona
Av. Diagonal 645 Barcelona 08028 (Spain)
E-mail: esanudo@ub.edu

[b] Dr. J. R. Zuazo, Dr. G. R. Castro, Dr. E. Jiménez
BM25 SpLine, and ID-08. ESRF
6 Rue Jules Horowitz, BP 220, 38043 Grenoble (France)

[c] S. Tewary, Dr. G. Rajaraman
Indian Institute of Technology, Mumbai (India)

[**] HOPG = Highly ordered pyrolitic graphite.

Supporting information for this article is available on the WWW under http://dx.doi.org/10.1002/chem.201402814.

show that for the Mn_{12} SMMs[9] the molecules do not remain intact after deposition, usually presenting reduction to Mn^{II} and decomposition, with the loss of the SMM property. The reported data are far better for the Fe_4 SMMs, which are robust molecules that can be deposited intact on a surface, maintaining the SMM property.[10] Thus, deposition methods for molecular systems greatly depend on the nature of the molecule and its functional groups. As chemists, the main challenges we face are the design and synthesis of new functional nanomagnets that are robust and can be processed without suffering decomposition. This is the key to being able to use these molecular systems in technological devices in the not-so-distant future. In this paper we report our latest results in this direction: The new fluorescent ligand **ACRI-1** and its Co^{II} complex [Co_2(**ACRI-1**)$_2$] (**1**) are presented. The new fluorescent complex **1** has been characterized in bulk and as thin films on a HOPG surface.

Results and Discussion

We have designed and prepared the fluorescent ligand **ACRI-1** based on acridine yellow through Schiff base formation with salicylaldehyde.[11] **ACRI-1** is a ditopic ligand with two separate coordination pockets that are far enough to avoid quenching of the fluorescence of the central fluorophore by coordination to a metal atom. The fluorescent properties of **ACRI-1** and its complexes are derived from the fluorescent group acridine yellow. Treatment of **ACRI-1** with Co^{II} nitrate hexahydrate afforded a precipitate that was recrystallized in chloroform to afford dark-red crystals of complex **1**, [Co_2(**ACRI-1**)$_2$], in 25% yield.

Description of the crystal structures

Table 1 contains the crystallographic data and structural parameters for **ACRI-1** and complex **1** (see the Supporting Information for additional crystallographic parameters). The ligand **ACRI-1** crystallizes in the monoclinic space group $C2/c$ and the crystal structure is shown in Figure 1. The crystal structure shows the intramolecular hydrogen bond between the oxygen atom of the phenol group and the iminic nitrogen. Complex
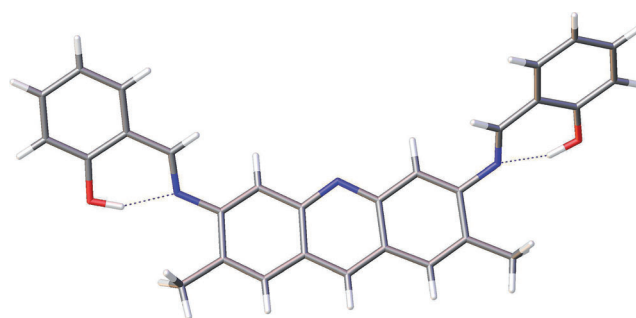

Figure 1. Crystal structure of the ligand **ACRI-1**. Intramolecular OH⋯N hydrogen bonds are shown as dashed lines.

1 crystallizes in the triclinic space group $P\bar{1}$. The crystal structure and packing diagrams are shown in Figure 2. In [Co_2-(**ACRI-1**)$_2$] (**1**) the Co^{II} atoms are tetracoordinated in a distorted tetrahedral environment. The asymmetric unit contains two half molecules (Co1 and Co2) with a torsion angle Co1-Co1′⋯Co2-Co2′ of 112° (Co1′ and Co2′ are the symmetry related atoms to Co1 and Co2), these are shown in green and blue in the packing diagram of Figure 2. The intramolecular Co–Co′ distances are Co1–Co1′ 12.015 and Co2–Co2′ 11.901 Å. Between different molecules the Co^{II}–Co^{II} distances range between 12.168 and 8.069 Å. The acridine core of the ligand **ACRI-1** displays parallel-displaced intramolecular π–π stacking. The average distance between the aromatic rings is 3.5 Å. Between molecules with the same symmetry there are several

Table 1. Crystal data and structure refinement parameters for **ACRI-1** and complex **1**.

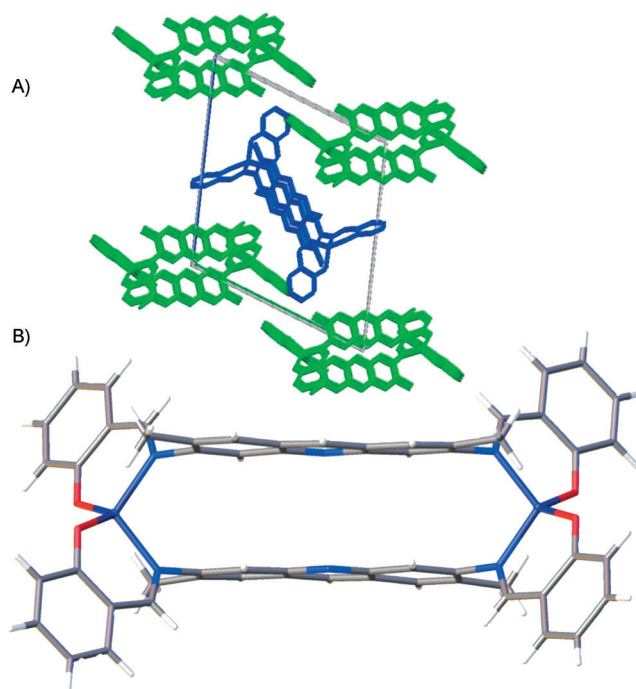| Sample	ACRI-1	Complex 1
crystal system	monoclinic	triclinic
space group	$C2/c$	$P\bar{1}$
a [Å]	27.571(3)	10.0214(5)
b [Å]	4.8628(6)	17.8460(9)
c [Å]	33.133(4)	18.2959(9)
α [°]	90.00	104.780(2)
β [°]	101.759(7)	102.115(2)
γ [°]	90.00	106.115(2)
V [Å³]	4348.9(9)	2897.4(3)
Z	8	2
final R indexes	$R_1 = 0.0634$	$R_1 = 0.0504$
[$I > 2\sigma(I)$]	$wR_2 = 0.1317$	$wR_2 = 0.1487$

Figure 2. a) Crystal structure of one of the two isostructural dinuclear units that compose the asymmetric unit of complex **1**; b) Packing diagram in which the two crystallographically independent dinuclear units of complex **1** are shown in green and blue.

types of interaction: π–π stacking between salicylaldehyde rings with average distance of 3.346 Å, π–π stacking between anthracene and salicylaldehyde rings with average distances of 3.321 Å, and H-bonds between the oxygen of the phenoxy group of one molecule with a C–H of salicylaldehyde ring of the neighbor, O2–C31′ C31–O2′ at 3.377 Å.

Between molecules with different symmetry the interactions are π–π stacking between anthracene rings, and between salicylaldehyde rings with distances between 3.698 and 3.309 Å. In addition there are H-bonds between the oxygen of the phenoxy group and a C–H of the salicylaldehyde ring O3–C54′′ at 3.588 Å, and the nitrogen of the anthracene and a C–H of the salicylaldehyde ring N3–C25′′ at 3.375 Å. These distances are in agreement with the expected for weak CH–X hydrogen bonds.[12] The interactions repeat over the crystal packing and even though they are weak by themselves, cooperatively they are of vital importance for the magnetic properties of complex 1. The intermolecular interactions can be easily visualized calculating the Hirshfield surface,[13] see the Supporting Information for a Figure that shows that the points of maximum intermolecular interaction, shown in red, are those close to the first coordination sphere of the Co^{II} ions.

Fluorescent properties

Emission spectra of ligand ACRI-1 and complex 1 are shown in Figure 3 at an excitation wavelength of 350 nm. In all cases a peak corresponding to excimer formation of the acridine core is observed at about 550 nm. Dilution to 10^{-9} M of ACRI-1 is necessary to observe the fluorescence of the ligand, which is blueshifted to 425 nm, as usual for anthracene and pyrene derivatives.[14] The emission spectrum of complex 1 shows the expected intramolecular excimer emission around 550 nm at all concentrations, which suggests that the molecule remains stable in solution. The coordination of Co^{II} does not suppress the fluorescence of the ACRI-1 ligand. However, a quenching of the fluorescence is observed, resulting in less intense signals. The fluorescence spectrum of complex 1 shows no traces of free ligand, supporting the stability of complex 1 in solution as observed by NMR spectroscopy (see below).

Stability of complex 1 in solution

To deposit complex 1 from solution onto a substrate, its stability under the treatment conditions must be established without question. The solution stability of complex 1 can be assessed by means of mass spectroscopy and paramagnetic proton NMR spectroscopy. The ESI mass spectrum of complex 1 shows the molecular ion peak at $m/z = 1006$. However, under the conditions of the electrospray, complex 1 fragments easily and the most important signals are the peaks for ACRI-1 ($m/z = 446$) and acridine yellow from ligand fragmentation ($m/z = 238$). A solution of complex 1 in deuterated chloroform was prepared and its proton NMR spectrum studied over time. The NMR spectrum did not change over long periods of
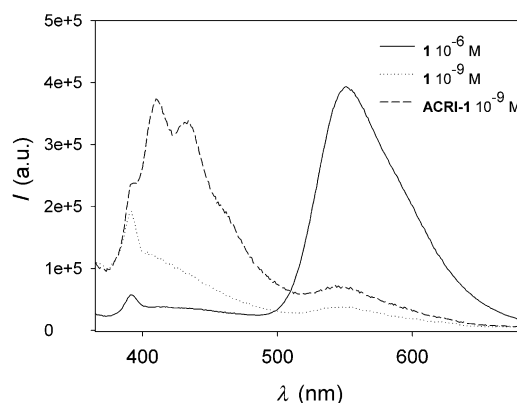

Figure 3. Emission spectra of complex 1 (1×10^{-9} and 1×10^{-6} M) and the free ligand ACRI-1 (1×10^{-9}) at an excitation wavelength of 350 nm. The data for complex 1 at 1×10^{-6} has been divided by 20 to fit in the scale.

time of up to one day. The proton NMR spectrum of solid samples kept at room temperature, open to air, did not change over long periods of time (several months to one year), thus the bulk solid is stable and no oxidation of Co^{II} to Co^{III} due to atmospheric oxygen occurs. The proton NMR spectrum of complex 1 is shown in Figure 4, with the signals assigned to the respective protons as indicated. The simple NMR spectrum clearly shows that the complex is stable in solution and that the ligand remains coordinated to the complex. The solution can be driven to dryness by evaporation of the CDCl$_3$ and then the solid re-dissolved in deuterated chloroform again: No changes are observed in the spectrum. The proton NMR spectrum of the precipitate, as obtained from the reaction, without further treatment, is that of complex 1, with a small amount of free ligand. Treatment of this precipitate at 200 °C for 2 h in an oven results in the elimination of the free ligand and a residue of pure complex 1, as analyzed by proton NMR spectroscopy. Thus the NMR spectroscopy and mass spectrometry, together with the fluorescence analysis of complex 1 in solution, show that it is stable and further processing using a solution of the complex can be pursued.
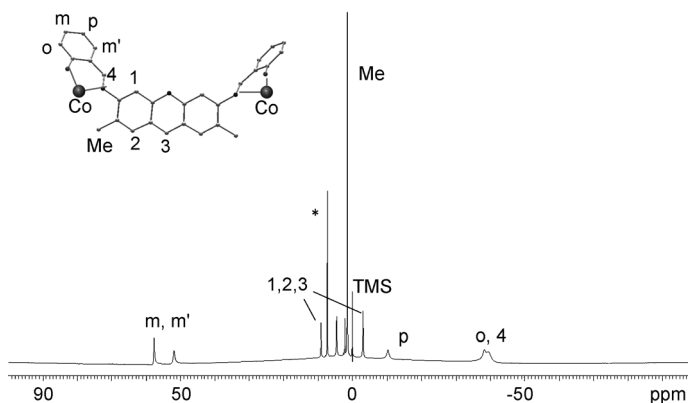

Figure 4. Proton NMR spectrum of complex 1 in deuterated chloroform.

Bulk magnetic properties

The magnetic susceptibility of **1** was investigated in the temperature range 2–300 K at applied fields of 300 and 5000 Oe. The plot of $\chi_M T$ versus T is shown in Figure 5. Upon cooling, the $\chi_M T$ value is nearly constant down to 60 K. Below this tem-
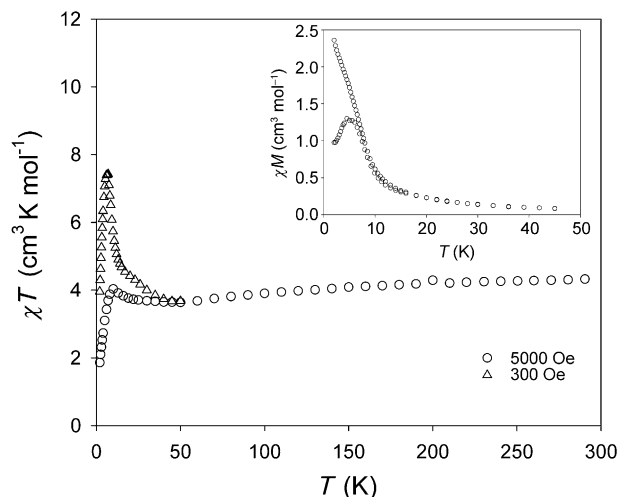

Figure 5. Direct current (dc) magnetic susceptibility data for complex **1** shown as a χT versus T plot at 5000 and 300 Oe, and zero-field cooling/field cooling plot at 300 Oe (inset).

perature the $\chi_M T$ product increases to 4.06 cm^3 mol^{-1} K at 15 K. Below 15 K the $\chi_M T$ product drops to a value of 1.85 cm^3 mol^{-1} K at 2 K. The $\chi_M T$ value 4.31 cm^3 K mol^{-1} at 300 K is in agreement with the calculated value of 3.75 cm^3 K mol^{-1} for two magnetically isolated distorted tetrahedral Co^{II} atoms ($S = 3/2$, $g = 2.0$). Alternating current (ac) magnetic susceptibility data of complex **1** were collected at different frequencies of an oscillating ac field of 4 Oe. A signal is observed in the out-of-phase susceptibility with a maximum at 5 K indicating the onset of ferromagnetic order. This long-range interaction is promoted by the intermolecular interactions in the 3D network of complex **1**, as discussed before. The peak in the out-of-phase ac magnetic susceptibility has a maximum at 5 K, and the zero-field cooling/field cooling (ZFC-FC) measurement shows a splitting of the two curves at this same temperature (as shown in the inset of Figure 5) indicating that 5 K is the blocking temperature for the ferromagnetic order of complex **1**. Many molecular magnets based on Co^{II} are reported in the literature. Usually, mononuclear tetrahedral Co^{II} complexes with weaker intermolecular interactions than those found in complex **1** order at temperatures below 2 K,[15] whereas the tridimensional coordination polymer [Co(dca)$_2$] (dca = dicyanamide) has ferromagnetic order at 9 K.[16]

Theoretical studies on complex 1

The X-ray structure was treated as an initial guess to perform the quantum chemical calculations for both intra- and intermolecular interactions in complex **1**. The DFT[17] calculations using the Gaussian 09 suite of programs[18] were carried out to yield the single-point energies of all possible electronic states (see the Supporting Information for details). The single-point computed structure of the tetramer has been shown in Figure 6. The magnetic exchange interactions were calculated for complex **1** to underpin the mode of coupling between the two tet-
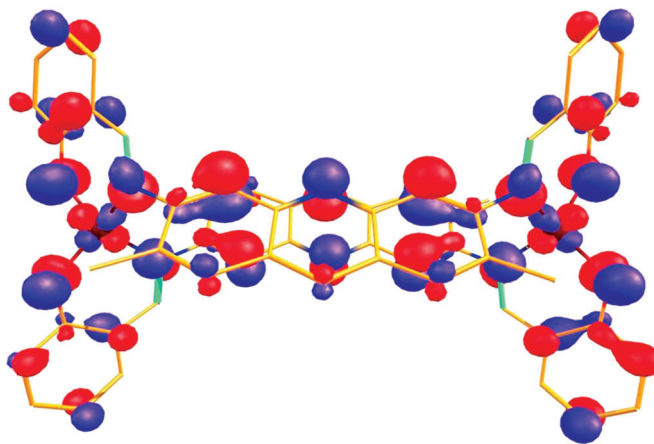

Figure 6. Highest occupied molecular orbital (HOMO) of complex **1**.

rahedral Co^{II} ions mediated through an extended aromatic ring system. DFT calculations reveals that both the intra- and interdimer exchange interactions are ferromagnetic in nature with J value of 0.15 and 0.03 cm^{-1}, respectively. The computed values are in good agreement to the experimental observation. The magnitude of intramolecular exchange is relatively weak, essentially due to the long distance between the two Co^{II} centers. The inter-dimer exchange is much weaker as the exchange interactions are mediated through H-bonding interactions. The spin density plots are shown in Figure 6. In all cases the spin density on the Co^{II} atom are about 2.7 suggesting significant delocalization of spin density to other atoms. Particularly the coordinated N- and O-donor atoms have significant positive spin density due to spin delocalization. Particularly, on coordination nitrogen spin density of ≈ 0.05 has been detected and this is in accord with the XAS N-edge spectra discussed below. One of the magnetic orbitals (highest occupied molecular orbital; HOMO) of **1** is shown in Figure 6 as the unpaired electrons in Co^{II} are present in t$_2$ set of orbitals possessing σ-character and this promotes spin delocalization to the coordinating atoms (see the Supporting Information for the computed Eigen value plot for complex **1**). From the coordinating atoms spin polarization propagates as evidence from the alternating spin densities on the spacer atoms. Significant contributions from ACR-I ligand to the HOMO reveals that observed exchange is super-exchange in nature through the aromatic spacer ligands. The ferromagnetic coupling is essentially related to the metal–metal distance and number of the spacer groups/atoms. An earlier prediction of long-range coupling on the Cu^{II} complex suggest that the exchange should be ferromagnetic in this case as there are three aromatic spacer groups.[19]

Surface deposition and characterization

To study the surface deposition, a 10^{-5} M solution of complex **1** in acetone was deposited onto freshly cleaved HOPG by spin coating at 500 rpm during 30 seconds. Clean acetone was deposited on HOPG by spin coating in the same conditions as those used to prepare the sample of complex **1** and the AFM showed a pristine HOPG surface. The topography of the samples was characterized by atomic force microscopy (AFM) using peak force mode. Figure 7 shows two AFM images of a thin-layer of complex **1** with an average height of 1.2 nm. The observed 1.2 nm height of the layer fits with the height of the molecule when it is placed with the salicylaldehyde groups interacting by π–π stacking with the HOPG surface. A TOF-SIMS experiment was performed to see in complex **1** was deposited and remained intact under the deposition conditions. The surface used was conductive Si, since the TOF-SIMS technique requires a conductive surface. The samples were prepared under the same spin-coating conditions used to prepare the samples for AFM, one was studied by TOF-SIMS and the other by AFM. The AFM revealed a continuous coverage of the surface with aggregates with heights of around 1 to 2 nm distributed on the surface. The TOF-SIMS spectra (see the Supporting Information) showed peaks at $m/z = 446$ and 488, which can be associated to the [(**ACRI-1**)+H]$^+$ and [Co(**ACRI-1**)-Me]$^-$ fragments, and the presence of Cobalt in the deposited layer, confirming that the aggregates observed in the AFM images correspond to molecules of complex **1**, which had been deposited intact on the surface. Grazing incidence X-ray diffraction (GIXRD) was performed on a spin-coated HOPG sample, prepared in the same conditions as the AFM samples, and compared to that of a pellet of bulk complex **1**. Unfortunately, the diffraction features observed were very weak due to the extremely low quantity of material of the monolayer and the very strong diffraction signals of the polycrystalline HOPG substrate. A saturated solution of complex **1** was drop-casted on a glass plate and a GIXRD of the thin film was then measured; it showed a weak diffraction pattern like that of the pellet of bulk complex **1**, (see the Supporting Information).

Thus, polycrystalline thin layers of complex **1** can be deposited on a surface. In the GIXRD of the spin-coated HOPG, some diffraction peaks observed over long acquisition times coincided with those of the bulk sample of **1** and the drop-casted **1** on glass. Bulk complex **1** and thin films of complex **1** on HOPG were studied by X-ray absorption spectroscopy (XAS) at ESRF beamline ID-08. XAS spectra were taken at both Co- and N-edge. The X-ray magnetic circular dichroism (XMCD) spectra is defined by the difference between the absorption spectra collected with left and right polarized light. XAS spectra and the dichroic signal at Co-edge for a thin layer of complex **1** on HOPG and a powder sample of complex **1** are shown in Figure 8. A full study was performed varying the field and temperature down to 10 K, both the powder of complex **1** and the thin layer of complex **1** on HOPG displayed a paramagnetic signal. Unfortunately, a temperature of 10 K is above the blocking temperature of the ferromagnetic order of complex **1**, thus we have been unable to establish whether the thin layer of complex **1** displays long-range magnetic order as the bulk sample does. Clearly the spectra of complex **1** on HOPG is very similar to that of bulk complex **1**, proving that complex **1** is intact after deposition on HOPG by spin coating. A simulation of the spectrum with the software CTM4XAS[20] is also shown in Figure 8. The software performs atomic multiplet calculations and allows the crystal field parameters to be adjusted. The spectral features observed both for complex **1** and complex **1** on HOPG can be simulated with crystal field parameters in agreement with those expected for distorted tetrahedral Co^{II} in a coordination environment like that found in complex **1**. It has been found that in both cases the spectral are well simulated for Co^{II} in a distorted tetrahedral environment. The crystal field parameters used in the simulation are 10Dq, which is the crystal field splitting of the d orbitals (in the program a negative value is used for tetrahedral crystal field), Dt and Ds, which reflect the distortion with respect to an ideal environment. The best simulation of XAS and XMCD spectra was obtained for 10Dq = 0.63 eV (5081 cm^{-1}), Dt = 0.025 and Ds = −0.15 for the powder complex **1** sample and 10Dq = 0.70 eV (5645 cm^{-1}), Dt = 0 and Ds = −0.2 for the thin layer of complex **1** on HOPG,
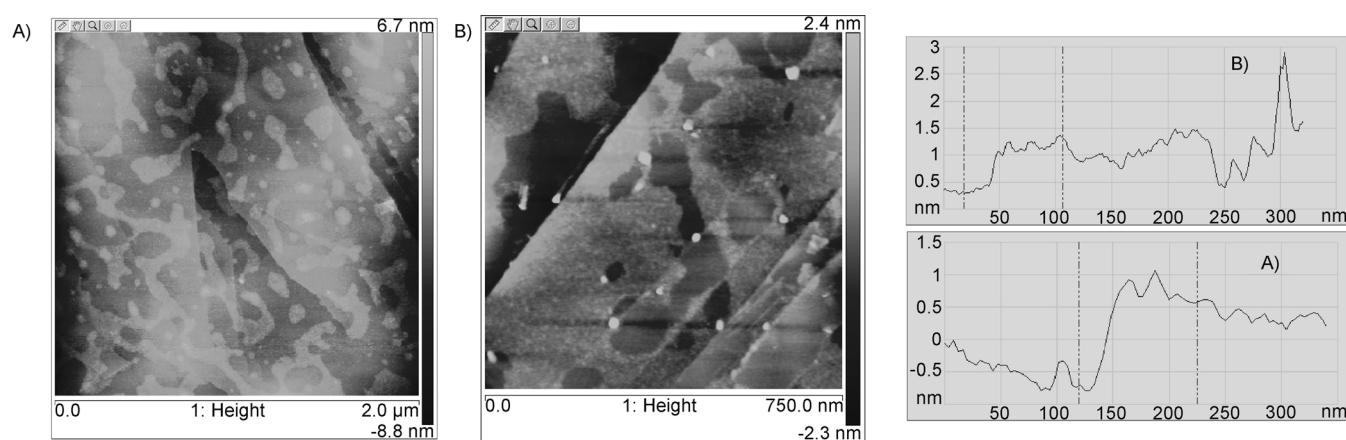

Figure 7. AFM images A) 2 μm image and B) 50 nm image and depth profiles of two samples of a solution of complex **1** (1×10^{-5} M) deposited by spin-coating on HOPG.
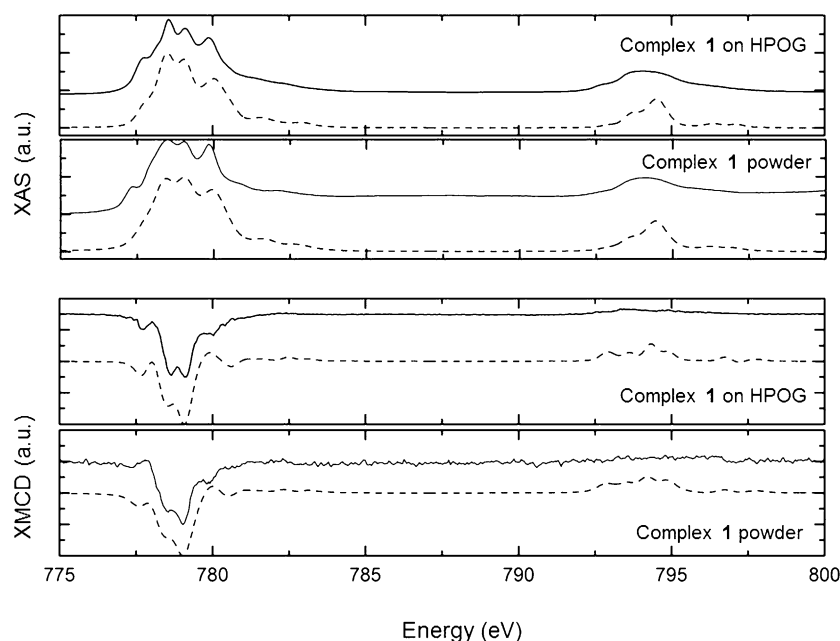
Figure 8. X-ray absorption (XAS) and X-ray magnetic circular dichroism plots for a thin layer on complex **1** deposited on HOPG by spin coating (complex **1** on HOPG) and a bulk sample of complex **1** (complex **1** powder). The dashed lines are simulations calculated using CTM4XAS (see the text for the simulation parameters).

and these are shown as dashed lines in Figure 8. The 10Dq values obtained are in agreement with the expected 10Dq values for tetrahedral Co^{II} with N and O donors.[21] At N-edge, and XLD signal was measured presenting a maximum at 45 degrees from the plane of the surface, in agreement with the DFT calculations that suggest that there is unpaired electron density on the N atoms of the **ACRI-1** ligand.

Conclusion

We have presented here the new multifunctional material [Co$_2$-(**ACRI-1**)$_2$] (**1**) with fluorescent and magnetic properties. The stability of the complex has been established and surface deposition studies performed. The fluorescent complex **1** can be deposited intact on a surface, as shown by XAS. The XAS and XMCD spectra of complex **1** can be modeled with crystal field parameters in agreement with the crystal structure of the molecule. The N-edge measurements suggest a preferential orientation of the molecules on the HOPG surface. For possible applications of nanomagnets in devices, this is a key point that still needs to be carefully assessed, especially when the nanomagnets in question are polynuclear coordination complexes.

Experimental Section

All chemicals were purchased from commercial sources and used as received.

C$_{29}$H$_{23}$N$_3$O$_2$ (ACRI-1): Salicylaldehyde (931 µL, 8.89 mmol) was added to a mixture of acridine yellow hydrochloride (C$_{15}$H$_{16}$N$_3$Cl; 1.215 g, 4.45 mmol) and triethylamine (3.10 mL, 22.23 mmol) in ethanol (100 mL). The resulting solution was stirred and heated up to 79 °C and was heated at reflux for 8 h. After standing overnight,

a precipitate was filtered, washed with ethanol, and dried with diethyl ether. The yield of the reaction was 73% (1.45 g). Suitable crystals for single-crystal X-ray diffraction were grown from concentrated acetonitrile solution by slow evaporation. Selected IR data (KBr): $\tilde{v} =$ 3310.72 (m), 3196.04 (s), 1645.65 (s), 1569.05 (m), 1504.37 (s), 1460.63 (m), 1388.36 (m), 1353.19 (m), 1185.98 (m), 1130.18 (m), 847.79 (m), 759.94 (w), 635.00 cm^{-1} (w); elemental analysis calcd (%) for C$_{29}$H$_{23}$N$_3$O$_2$·1/2 H$_2$O: C 76.62; H 5.32; N 9.24; found: C 76.6; H 5.06; N 9.14.

[Co$_2$(ACRI-1)$_2$] (1): A solution of the ligand **ACRI-1** (C$_{29}$O$_2$N$_3$H$_{21}$; 0.25 g, 0.56 mmol) in acetonitrile (20 mL), was treated with [Co(NO$_3$)$_2$]·6 H$_2$O (0.16 g, 0.56 mmol) and three equivalents of Et$_3$N (240 µL, 1.68 mmol). After 24 h of stirring a precipitate was filtered, washed with acetonitrile, and dried with anhydrous diethyl ether. Yield: 25% (0.14 g). Slow diffusion of hexanes into a chloroform solution of the precipitate results in the formation of single crystals of [Co$_2$(**ACRI-1**)$_2$] (**1**) suitable for X-ray diffraction. $M_w = 1006$ g mol^{-1}; ESI-MS: $m/z = 1006$; Selected IR data (KBr): $\tilde{v} = 3442.51$ (m), 3007.80 (s), 1605.03 (s), 1575.30 (s), 1528.98 (s), 15 1494.80 (m), 1456.99 (s), 1435.93 (s), 1383.90 (m), 1321.39 (m), 1276.09 (m), 1184.57 (m), 1151.53 (m), 1131.64 (s), 915.23 (m), 869.03 (m), 752.90 (s), 635.49 (m), 577.47 cm^{-1} (w); elemental analysis calcd (%) for C$_{66}$H$_{72}$Co$_2$N$_{10}$O$_{13}$: C 59.53, H 5.45, N 10.52; found: C 59.79, H 4.78, N 10.20.

Single-crystal diffraction data were collected on a Bruker APEXII SMART diffractometer at the Facultat de Química, Universitat de Barcelona, using a microfocus Molybdenum K$_\alpha$ radiation source. The structures were solved by direct methods (SHELXS) and refined on F^2 (SHELX). CCDC-917646 (**ACRI-1**) and CCDC-917647 (**1**) contain the supplementary crystallographic data for this paper. These data can be obtained free of charge from The Cambridge Crystallographic Data Centre via www.ccdc.cam.ac.uk/data_request/cif. IR, UV/Vis, and fluorescence spectra were recorded at the in-house facilities. Elemental analyses, magnetic measurements (SQUID magnetometer equipped with a 5 T magnet on crushed crystals) and ^{1}H NMR spectroscopy (Varian Unity 300 MHz) were performed at the CCiT-UB. Surface characterization was done at the CCiT-UB by using an AFM Multi mode. The electronics of the system are Nanoscope V from Bruker. Topographic mode: peak force. Each image has a resolution of 512×512 pixels, taken at a velocity of 1 row/s. Tip used: silicon oxide with a nominal radius of 5 nm. The X-ray diffraction experiment at grazing incidence angle was carried out at a fixed wavelength of 0.826 Å on a six-circle diffractometer, using a 2D-charge coupled device (Photonic Science CCD) detector, at SpLine beamline (BM25B), ESRF, Grenoble, France. The detector has an active area of 250×125 mm^2 and 60 3825×1913 (2×2 binned) pixels, with a 65.6 micron pixel size. The sample–detector distance during the experiment varied from 180 up to 630 mm. The X-ray magnetic circular dichroism (XMCD) measurements have been performed at the beamline ID08 at ESRF, which is based on Apple II

undulator source allowing a full control of linear and circular polarization and a high scanning speed spherical grating monochromator Dragon type. The absorption signal has been measured in total electron yield at 10 K. A magnetic field parallel to the incident beam was provided by a superconducting electromagnet.

Computational details

The magnetic exchange coupling constant (J) was evaluated by employing the Noodleman's broken symmetry approach, as developed by Ginsberg and Noodleman.[22] The hybrid B3LYP functional,[23] which is known to better reproduce the numerical estimates of magnetic exchange especially for transition-metal complexes have been used for our calculations. Ahlrichs triple-ζ valence basis set (TZV)[24] employed over all the elements to have better understanding in terms of the energies and spin densities. Molekel version 4.3 has been used to generate the spin density plots and Chemcraft version 1.6 has been used to visualize and represent the geometry of the complexes for this article.[25] For calculating magnetic susceptibility along with the relative spin state energies we have employed the MAGPACK software.[26]

[1] J. F. Gregg, I. Petej, E. Jouguelet, C. Denis, *J. Phys. D* **2002**, *35*, R121.

[2] S. Sanvito, *Nat. Mater.* **2007**, *6*, 803.

[3] J. Camarero, E. Coronado, *J. Mater. Chem.* **2009**, *19*, 1678.

[4] R. E. P. Winpenny, *J. Chem. Soc. Dalton Trans.* **2002**, 1.

[5] E. Coronado, D. Gatteschi, *J. Mater. Chem.* **2006**, *16*, 2685.

[6] A. Pons-Balagué, S. Piligkos, S. J. Teat, J. Sánchez Costa, M. Shiddiq, S. Hill, G. Castro, P. Ferrer-Escorihuela, E. C. Sañudo, *Chem. Eur. J.* **2013**, *19*, 9064.

[7] D. Gatteschi, A. Cornia, M. Mannini, R. Sessoli, *Inorg. Chem.* **2009**, *48*, 3408.

[8] a) M. Affronte, F. Troiani, A. Ghirri, S. Carretta, P. Santini, V. Corradini, R. Schuecker, C. Muryn, G. Timco, R. E. Winpenny, *Dalton Trans.* **2006**, 2810; b) A. Ghirri, V. Corradini, V. Bellini, R. Biagi, U. del Pennino, V. De Renzi, J. C. Cezar, C. A. Muryn, G. A. Timco, R. E. P. Winpenny, M. Affronte, *ACS Nano* **2011**, *5*, 7090.

[9] a) M. Mannini, Ph. Sainctavit, R. Sessoli, Ch. Cartier dit Moulin, F. Pineider, M. A. Arrio, A. Cornia, D. Gatteschi, *Chem. Eur. J.* **2008**, *14*, 7530; b) R.

[10] a) M. Mannini, F. Pineider, P. Sainctavit, C. Danieli, E. Otero, C. Sciancalepore, A. M. Talarico, M.-A. Arrio, A. Cornia, D. Gatteschi, R. Sessoli, *Nat. Mater.* **2009**, *8*, 194; b) M. Mannini, F. Pineider, C. Danieli, F. Totti, L. Sorace, Ph. Sainctavit, M.-A. Arrio, E. Otero, L. Joly, J. C. Cezar, A. Cornia, R. Sessoli, *Nature* **2010**, *468*, 417.

[11] D. Reta Mañeru, M. J. Heras Ojea, L. Rosado, G. Aromí, J. Zuazo, G. Castro, E. C. Sañudo, *Polyhedron ICMM 2012 proceedings*, **2013**, in press.

[12] W. C. Hamilton, J. C. Ibers, *Hydrogen Bonding in Solids* (Ed: W. A. Benjamin), New York, **1968**.

[13] a) J. J. McKinnon, M. A. Spackman, A. S. Mitchell, *Acta Crystallogr. B* **2004**, *60*, 627; b) F. L. Hirshfeld, *Theor. Chim. Acta* **1977**, *44*, 129.

[14] T. Seko, K. Ogura, Y. Kawakami, H. Sugino, H. Toyotama, J. Tanaka, *Chem. Phys. Lett.* **1998**, *291*, 438.

[15] M. C. Moron, F. Palacios, J. Pons, J. Casabó, R. L. Carlin, *J. Solid State Inorg. Chem.* **1991**, *28*, 431.

[16] S. R. Batten, P. Jensen, B. Moubaraki, K. S. Murray, R. Robson, *J. Chem. Soc. Chem. Commun.* **1998**, 439.

[17] F. Jensen, *Introduction to Computational Chemistry*, 2ednd edJohn Wiley & Sons, Chichester, **2007**.

[18] Gaussian 09, Revision A.02, M. J. Frisch, G. W. Trucks, H. B. Schlegel, G. E. Scuseria, M. A. Robb, J. R. Cheeseman, G. Scalmani, V. Barone, B. Mennucci, G. A. Petersson, H. Nakatsuji, M. Caricato, X. Li, H. P. Hratchian, A. F. Izmaylov, J. Bloino, G. Zheng, J. L. Sonnenberg, M. Hada, M. Ehara, K. Toyota, R. Fukuda, J. Hasegawa, M. Ishida, T. Nakajima, Y. Honda, O. Kitao, H. Nakai, T. Vreven, J. A. Montgomery, Jr., J. E. Peralta, F. Ogliaro, M. Bearpark, J. J. Heyd, E. Brothers, K. N. Kudin, V. N. Staroverov, R. Kobayashi, J. Normand, K. Raghavachari, A. Rendell, J. C. Burant, S. S. Iyengar, J. Tomasi, M. Cossi, N. Rega, J. M. Millam, M. Klene, J. E. Knox, J. B. Cross, V. Bakken, C. Adamo, J. Jaramillo, R. Gomperts, R. E. Stratmann, O. Yazyev, A. J. Austin, R. Cammi, C. Pomelli, J. W. Ochterski, R. L. Martin, K. Morokuma, V. G. Zakrzewski, G. A. Voth, P. Salvador, J. J. Dannenberg, S. Dapprich, A. D. Daniels, Ö. Farkas, J. B. Foresman, J. V. Ortiz, J. Cioslowski, D. J. Fox, Gaussian, Inc., Wallingford CT, **2009**.

[19] E. Pardo, J. Faus, M. Julve, F. Lloret, M. Carmen, J. Cano, X. Ottenwaelder, Y. Journaux, R. Carrasco, G. Blay, I. Fernandez, R. Ruiz, *J. Am. Chem. Soc.* **2003**, *125*, 10770.

[20] E. Stavitski, F. M. F. de Groot, *Micron* **2010**, *41*, 687.

[21] a) F. A. Cotton, D. M. L. Goodgame, M. Goodgame, *J. Am. Chem. Soc.* **1961**, *83*, 4690; b) D. W. Herlocker, R. S. Drago, *Inorg. Chem.* **1968**, *7*, 1479; c) S.-I. Aizawa, S. Funahashi, *Inorg. Chem.* **2002**, *41*, 4555.

[22] L. Noodleman, C. Y. Peng, D. A. Case, J. M. Mouesca, *Coord. Chem. Rev.* **1995**, *144*, 199.

[23] a) A. D. Becke, *J. Chem. Phys.* **1986**, *84*, 4524; b) J. P. Perdew, *Phys. Rev. B* **1986**, *33*, 8822.

[24] a) A. Schäfer, H. R. Horn, R. Ahlrichs, *J. Chem. Phys.* **1992**, *97*, 2571; b) A. Schäfer, C. Huber, R. Ahlrichs, *J. Chem. Phys.* **1994**, *100*, 5829.

[25] Molekel, Advanced Interactive 3D-Graphics for Molecular Sciences; http:\\www.cscs.ch/molkel/.Version 1.6(build 338), Programming Zhurko, G. A.; http://www.chemcraftprog.com.

[26] a) J. J. Borrás-Almenar, J. M. Clemente-Juan, E. Coronado, B. S. Tsukerblat, *Inorg. Chem.* **1999**, *38*, 6081; b) J. J. Borrás-Almenar, J. M. Clemente-Juan, E. Coronado, B. S. Tsukerblat, *J. Comput. Chem.* **2001**, *22*, 985.